NAD(H)-loaded nanoparticles for efficient sepsis therapy via modulating immune and vascular homeostasis

Mingzhou Ye[1,2,3,5], Yi Zhao[1,2,3,5], Yuyuan Wang[1,2,3], Ruosen Xie [1,2,3], Yao Tong[1,2,3], John-Demian Sauer[4] and Shaoqin Gong [1,2,3 ✉]

Sepsis is a life-threatening organ dysfunction responsible for nearly 270,000 deaths annually in the United States alone. Nicotinamide adenine dinucleotide (NAD⁺), an immunomodulator, can potentially treat sepsis; however, clinical application of NAD⁺ is hindered by its inability to be directly taken up by cells. To address this challenge, a family of nanoparticles (NPs) loaded with either NAD⁺ or the reduced form of NAD⁺ (NADH), hereafter NAD(H)-loaded NPs, were engineered to enable direct cellular transport and replenishment of NAD(H). The NAD(H)-loaded NPs improved cellular energy supply, suppressed inflammation and prevented inflammation-induced cell pyroptosis and apoptosis. Therefore, the NPs can help maintain immune homoeostasis and vascular function, two key factors in the pathogenesis of sepsis. The NAD(H)-loaded NPs demonstrated excellent therapeutic efficacies in treating endotoxemia and multidrug-resistant pathogen-induced bacteremia. In addition, the NAD(H)-loaded NPs prevented caecal ligation and puncture-induced multiorgan injury and improved outcomes of secondary *Pseudomonas aeruginosa* infections following caecal ligation and puncture, thus potentially leading to a highly innovative and translational approach to treat sepsis efficiently and safely.

Sepsis is a complex disorder caused by a dysregulated host response to infection, with high levels of morbidity and mortality[1]. Pathogen-induced hyperinflammation and subsequent immunosuppression as well as endothelial damage are the dominant features responsible for the high modality of sepsis, which cannot be adequately addressed by current therapeutic strategies such as broad-spectrum antibiotic therapy or fluid resuscitation[2,3]. Hence, there is an avid need to develop a new therapeutic strategy that can modulate the immune response and maintain vascular function.

NAD⁺ is known as an immune modulator[4]; however, its relationship to inflammation is not yet fully understood[5,6]. For instance, blocking NAD⁺ biosynthesis and supplying NAD⁺ precursors were both reported to downmodulate pro-inflammatory cytokine production[7,8]. A preprint paper published on BioRχiv reported that pre-injection of extremely high doses of NAD⁺ decreased mouse mortality to sepsis[9]. But there are also reports seemingly contradictory to this finding, suggesting that NAD⁺ or its precursor may not be beneficial to infections[10,11]. Therefore, the in vivo therapeutic benefit of NAD⁺ for sepsis is still under debate.

NAD⁺ is a negatively charged, hydrophilic small molecule that poorly diffuses across the cell membrane[12]. It has to be degraded extracellularly into its precursors, nicotinamide (NAM) or nicotinamide riboside (NR), to enter the cells and subsequently enhance NAD⁺ biosynthesis[13] (Fig. 1a). Such a limitation in NAD⁺ intracellular transport drastically decreases the bioactivity of NAD⁺ and necessitates an extremely high dose for effective therapy[10]. This may lead to inconsistent therapeutic outcomes and limit its potential for clinical translation. Furthermore, although NAM can enhance intracellular NAD⁺ biosynthesis, it can also induce the opposite effect of

NAD⁺ on a variety of important signals relevant to inflammation (for example, sirtuins and poly(ADP-ribose) polymerase (PARP))[14,15].

Several attempts were made to deliver NAD⁺ in vitro using nanovectors, but none was explored for in vivo applications due to undesirable drug loading and release profiles[16,17]. Here, we report a NAD⁺-loaded lipid-coated calcium phosphate (CaP) NP (NAD⁺-LP-CaP) and a NADH-loaded lipid-coated metal–organic framework (MOF) NP (NADH-LP-MOF), capable of directly replenishing the cellular NAD⁺ pool (Fig. 1a). The NAD(H)-loaded NPs enabled us, for the first time, to uncover the relationship between intracellular delivered NAD⁺ (instead of its precursors) and inflammation. These NPs, capable of directly delivering NAD(H) into the cytosol, are much stronger immune modulators compared with free NAD(H), and they prevented cell pyroptosis by blocking both canonical and non-canonical NACHT, LRR, and PYD domains-containing protein 3 (NLRP3) inflammasome pathways. In addition, the NAD(H)-loaded NPs improved cellular energy supply and inhibited cell apoptosis and dysfunction in immune cells and endothelial cells, thus preventing immune cell depletion and endothelial damage, two pivotal factors in the pathophysiology of sepsis[18,19]. Due to their strong ability in mitigating inflammation and balancing the immune and vascular homoeostases, the NAD(H)-loaded NPs showed striking therapeutic benefits in treating severe sepsis.

Formulation and characterization of the NAD(H)-loaded NPs
NAD⁺-LP-CaP was prepared using a water-in-oil reverse microemulsion method[20]. Dioleoylphosphatydic acid (DOPA) and ʟ-α-phosphatidylcholine (Soy PC) were used to form the inner and outer leaflet of the lipid bilayer, respectively, to stabilize

[1]Wisconsin Institute for Discovery, University of Wisconsin–Madison, Madison, WI, USA. [2]Department of Biomedical Engineering, University of Wisconsin–Madison, Madison, WI, USA. [3]Department of Ophthalmology and Visual Sciences, University of Wisconsin–Madison, Madison, WI, USA. [4]Department of Medical Microbiology and Immunology, University of Wisconsin–Madison, Madison, WI, USA. [5]These authors contributed equally: Mingzhou Ye, Yi Zhao. ✉e-mail: shaoqingong@wisc.edu
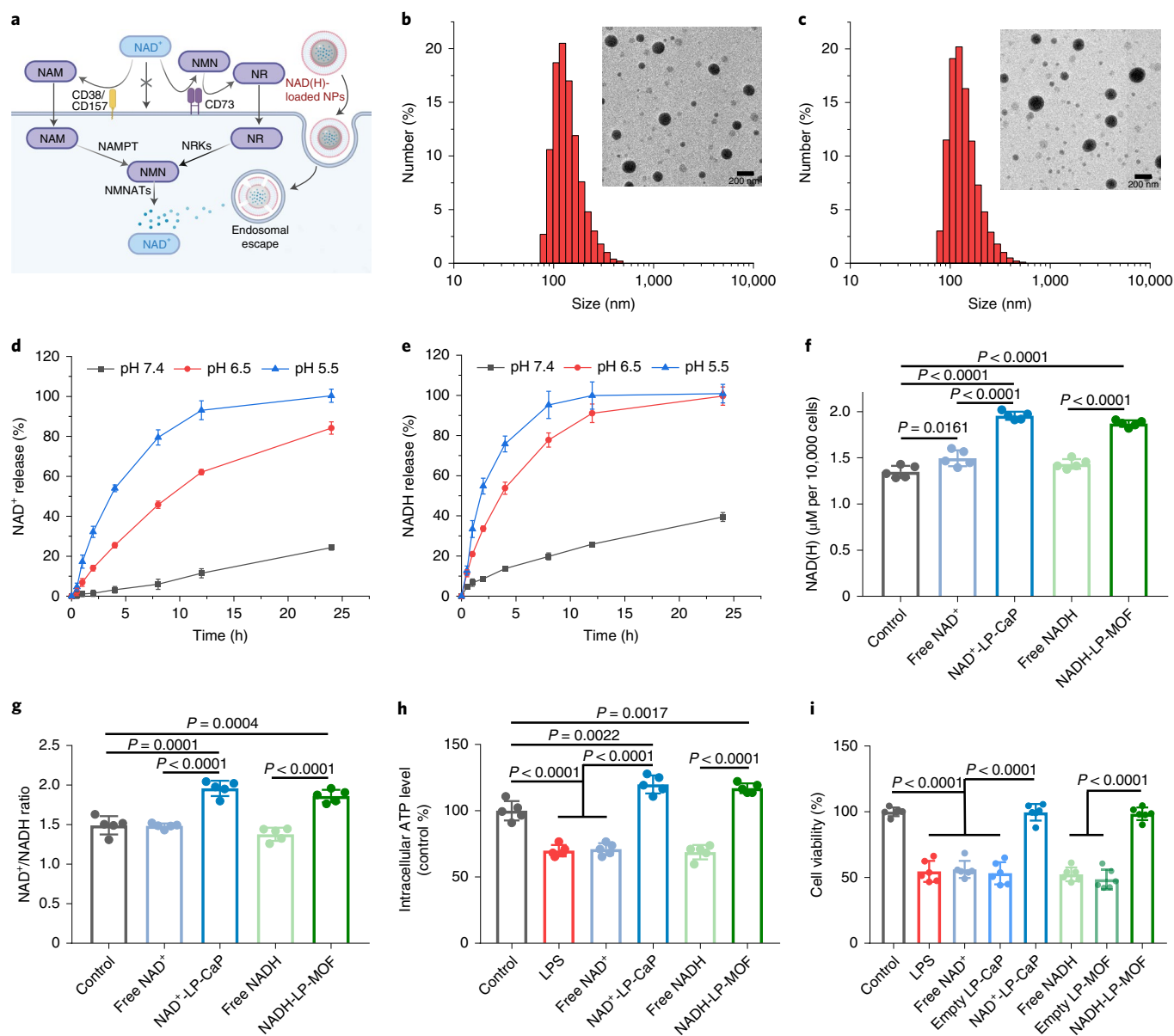
Fig. 1 | NAD(H)-loaded NPs replenished cellular NAD(H) pool and prevented inflammation-induced energy depletion. a, Schematic illustration of NAD^{+} metabolism and cellular uptake. Since NAD^{+} cannot pass through the cell membrane directly, it has to be degraded by extracellular enzymes into several precursors (for example, NAM and NR) which can enter the cells and subsequently enhance the NAD^{+} biosynthesis. Such a conversion process is inefficient as it is regulated and limited by critical enzymes (for example, NAMPT). The NAD(H)-loaded NPs can be taken up by the cells via endocytosis and directly replenish cellular NAD^{+}. The CaP or MOF cores can dissolve in acidic endosome, leading to endosome swelling and bursting (due to an increase in osmotic pressure) to release the entrapped payload into cytosol. Created with BioRender.com. NMN, nicotinamide mononucleotide; NMNAT, nicotinamide mononucleotide adenylyltransferase; NRK, nicotinamide riboside kinase. **b,c**, Size and morphology of NAD^{+}-LP-CaP (**b**) and NADH-LP-MOF (**c**) characterized by dynamic light scattering and transmission electron microscopy (inset). Representative data of three independent experiments. Scale bars, 200 nm. **d,e**, The NAD(H) release profiles from NAD^{+}-LP-CaP (**d**) and NADH-LP-MOF (**e**) under different pH values. Data are presented as mean ± s.d. ($n = 3$). **f,g**, Intracellular NAD(H) levels (**f**) and NAD^{+}/NAD(H) ratio (**g**) in BMDMs incubated with free NAD(H) (10 µM) or an equivalent dose of the NPs. Data are presented as mean ± s.d. ($n = 5$). Statistical significance was calculated via one-way analysis of variance (ANOVA) with Tukey's post hoc test. **h,i**, Quantification of intracellular ATP level ($n = 5$; **h**) and cell viability ($n = 6$; **i**) in an LPS-mediated energy depletion model. LPS-stimulated BMDMs (LPS, 100 ng ml⁻¹) were treated with free NAD(H) (10 µM) or an equivalent dose of the NPs. Data are presented as mean ± s.d. Statistical significance was calculated via one-way ANOVA with Tukey's post hoc test.

the NP. NADH-LP-MOF was prepared by mixing zinc nitrate, 2-methylimidazole and NADH in water to yield the zeolitic imidazolate framework 8 (ZIF-8) core, which was subsequently stabilized by a lipid coating via extrusion. Both NAD^{+}-LP-CaP and NADH-LP-MOF were spherical, and they had hydrodynamic diameters around 150 nm and 180 nm (Fig. 1b,c), respectively.

Both types of NPs were stable at 4 °C for one week. Lyophilized NPs maintained their stability for five weeks when stored at −20 °C (Supplementary Fig. 1). The loading efficiencies of NAD^{+}-LP-CaP and NADH-LP-MOF were 68.8% and 62.9%, respectively, and their loading contents were 12.4% and 5.2%, respectively. The NPs with pH-sensitive CaP and MOF cores demonstrated pH-responsive

NAD(H) release behaviours, which is desirable for this particular application (Fig. 1d,e). These NPs can prevent premature drug release in the bloodstream and protect NAD(H) from enzymatic degradation; however, they can quickly release NAD(H) in an acidic endosomal compartment and facilitate their endosomal escape via a proton sponge effect[21].

The NAD(H)-loaded NPs showed good biocompatibility (Supplementary Fig. 2) and were able to effectively replenish the cellular NAD(H) pool in multiple cell types (Fig. 1f and Supplementary Fig. 3). Both NAD$^+$-LP-CaP and NADH-LP-MOF significantly enhanced the intracellular NAD(H) levels in all four cell types investigated, ranging from 41% to 80%. By contrast, free NAD(H) showed a much weaker effect or no effect. While the NAD(H) level in the cells is quite high (~300 μM)[22], a much lower concentration of NPs in the cell culture media (containing 10 μM NAD(H)) effectively enhanced intracellular NAD(H) level.

The effect of the two types of NPs on the NAD$^+$/NADH ratio in bone-marrow-derived macrophages (BMDMs) was investigated since it is an important indicator of cellular metabolism and redox status. Interestingly, both NAD$^+$-LP-CaP and NADH-LP-MOF increased the NAD$^+$/NADH ratio (Fig. 1g). Cells can interconvert the extra NADH (delivered by NADH-LP-MOF) to NAD$^+$ through a set of redox systems, such as the tricarboxylic acid cycle, complex I of the electron transport chain and various cytosolic dehydrogenases, to maintain the NAD$^+$/NADH balance[12,23].

Inflammation and the resultant oxidative stress can trigger a unique metabolic status that consumes cellular NAD(H) quickly due to elevated PARP, sirtuin activations and CD38 expression[24,25]. The NAD(H)-loaded NPs effectively replenished the NAD(H) pool in the inflammatory cells and prevented NAD(H) loss induced by inflammation (lipopolysaccharide (LPS)), oxidative stress (hydrogen peroxide) and NAD$^+$ depletion (nicotinamide phosphoribosyltransferase (NAMPT) inhibitor FK866), while free NAD(H) did not show much benefit (Supplementary Fig. 4). NAD$^+$ is a key coenzyme participating in most energy-producing pathways in the cell, including glycolysis and oxidative phosphorylation. Therefore, maintaining NAD$^+$ homoeostasis is of great significance in preventing energy depletion and subsequent cell damage during inflammation[24]. The NAD(H)-loaded NPs enhanced the cellular ATP level in healthy cells and improved the ATP supply as well as cell viability for cells undergoing inflammation, oxidative stress or NAD$^+$ depletion (Fig. 1h,i and Supplementary Figs. 5 and 6).

## NAD(H)-loaded NPs prevent inflammation-induced cell death and dysfunction

Although NAD$^+$ is linked to inflammation, whether NAD$^+$ suppresses or fuels inflammation is still under debate[5–8]. To answer this question,

we treated the LPS-stimulated BMDMs with the NAD(H)-loaded NPs, and found that both NAD$^+$-LP-CaP and NADH-LP-MOF significantly reduced the production of pro-inflammatory cytokines TNF-α and IL-6 (Fig. 2a,b), thus demonstrating a strong anti-inflammatory effect induced by cytosolic delivery of NAD$^+$ or NADH. Empty NPs also slightly reduced cytokine production, consistent with the observation that lipid-coated NPs can absorb LPS, partially neutralizing its inflammatory effects[26]. By contrast, free NAD$^+$ and NADH did not show any anti-inflammatory effect.

Inflammasomes play a central role in activating inflammatory responses against infection[27]. Thus, the impact of the NAD(H)-loaded NPs on NLRP3 inflammasome activation was investigated. BMDMs were primed with LPS as signal 1 and then stimulated with ATP or Lipofectamine-2000-delivered LPS (lipoLPS) as signal 2 to activate 'canonical' and 'non-canonical' inflammasome pathways, respectively[28,29]. The NAD(H)-loaded NPs were added together with either signal 1 or signal 2 or both. Inflammasome activation was investigated by cell pyroptosis, caspase1 activation and IL-1β production. When co-incubated with either signal 1 or signal 2, the NAD(H)-loaded NPs led to a significant reduction in cell pyroptosis (Supplementary Figs. 7 and 8), caspase1 activation (Fig. 2c,d) and IL-1β production (Fig. 2e,f), demonstrating their ability to inhibit either the priming signal, the activation signal or both. Compared with the around 50% reduction in IL-1β release for the canonical pathway, the NPs completely blocked the IL-1β production and recovered the lactate dehydrogenase release to the baseline in the non-canonical pathway, demonstrating a more efficient suppression to this pathway. It was reported that pretreatment with 100 μM NAD$^+$ for two days could inhibit non-canonical inflammasome activation in BMDMs[9]. However, we did not observe this inhibition when adding free NAD(H) (10 μM) together with the stimuli. Such inconsistency might be attributed to the inefficient NAD$^+$ uptake by the cells.

To further investigate the effect of intracellular NAD$^+$ delivery to inflammasome gene transcription, nuclear factor kappa-light-chain-enhancer of activated B cells (NF-κB) p65 activation was observed by confocal laser scanning microscopy (CLSM). As shown in Fig. 2g,h, p65 nuclear translocation induced by LPS was decreased by both NAD$^+$-LP-CaP and NADH-LP-MOF treatments, consistent with previous studies on NAD$^+$ precursors, but with improved efficacy[25]. Moreover, the transcription levels of multiple inflammasome-related genes were significantly reduced by the NAD(H)-loaded NPs (Supplementary Fig. 9), which further corroborates with the NF-κB activation study. Apoptosis-associated speck-like protein containing a caspase recruitment domain (ASC) oligomerization triggered by signal 2 indicates NLRP3 inflammasome assembling and activation. The NAD(H)-loaded NPs

Fig. 2 | NAD(H)-loaded NPs prevented inflammation-induced cell death. a,b, Pro-inflammatory cytokine TNF-α (**a**) and IL-6 (**b**) levels in BMDM culture supernatant quantified by ELISA. LPS-stimulated BMDMs (LPS, 100 ng ml^{-1}) were treated with free NAD(H) (10 μM) or an equivalent dose of the NPs. Data are presented as mean ± s.d. ($n = 3$). Statistical significance was calculated via one-way ANOVA with Tukey's post hoc test. Statistical analyses were done relative to the LPS treatment group. **c–f**, Analysis of caspase1 activation (demonstrated by fluorochrome-labelled inhibitors of caspases (FLICA) probe 5-carboxyfluorescein-Tyr-Val-Ala-Asp-fluoromethylketone (FAM-YVAD-FMK) staining; $n = 5$; **c** and **d**) and IL-1β release ($n = 3$; **e** and **f**) indicating the activation of canonical (**c** and **e**) and non-canonical (**d** and **f**) inflammasome pathways. BMDMs were primed with LPS (100 ng ml^{-1}, 3 h) as signal 1, and then either incubated with ATP (2.5 mM, 1 h; for the canonical pathway) or transfected with lipoLPS (100 ng LPS per well, 3 h; for the non-canonical pathway) as signal 2. Free NAD$^+$, empty NPs (denoted as eCaP) or the NAD$^+$-LP-CaP NPs were added together with signal 1 or signal 2 or both. Data are presented as mean ± s.d. Statistical significance was calculated via one-way ANOVA with Tukey's post hoc test. Statistical analyses were done relative to the positive controls (LPS/ATP or LPS/lipoLPS). **g,h**, NF-κB p65 nuclear translocation observed by CLSM. BMDMs were pretreated with free NAD(H) or the NPs for 5 h, stimulated with LPS (100 ng ml^{-1}) for 1 h and then immunostained for p65. Representative images of five independent experiments. Scale bars, 20 μm. Data are presented as mean ± s.d. ($n = 5$). Statistical significance was calculated via one-way ANOVA with Tukey's post hoc test. Statistical analyses were done relative to the LPS treatment group. **i,j**, BMDM apoptosis triggered by LPS (100 ng ml^{-1}, 48 h) analysed by annexin V and propidium iodide double staining. FITC, fluorescein isothiocyanate. **k**, HUVEC apoptosis triggered by TNF-α (80 ng ml^{-1}, 48 h). The cells were treated with free NAD(H) or the NPs at a corresponding dose of 10 μM. **l**, Fluorescence images of HUVEC monolayer stained for tight junction protein VE-cadherin (green) after incubation with LPS together with free NAD(H) or the NPs for 24 h. Cell nuclei were stained by 4',6-diamidino-2-phenylindole (DAPI; blue). Representative images of three independent experiments. Scale bar, 50 μm.
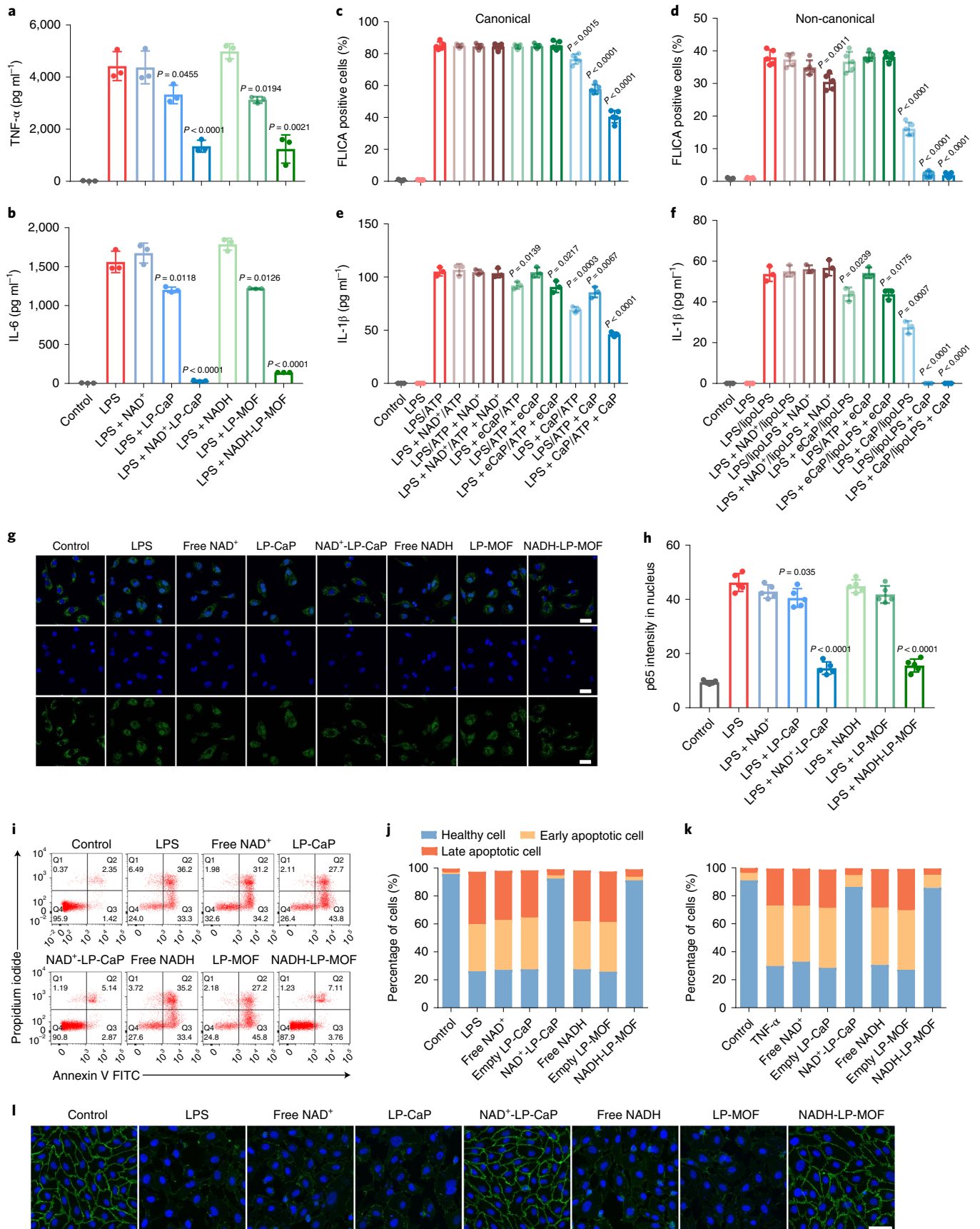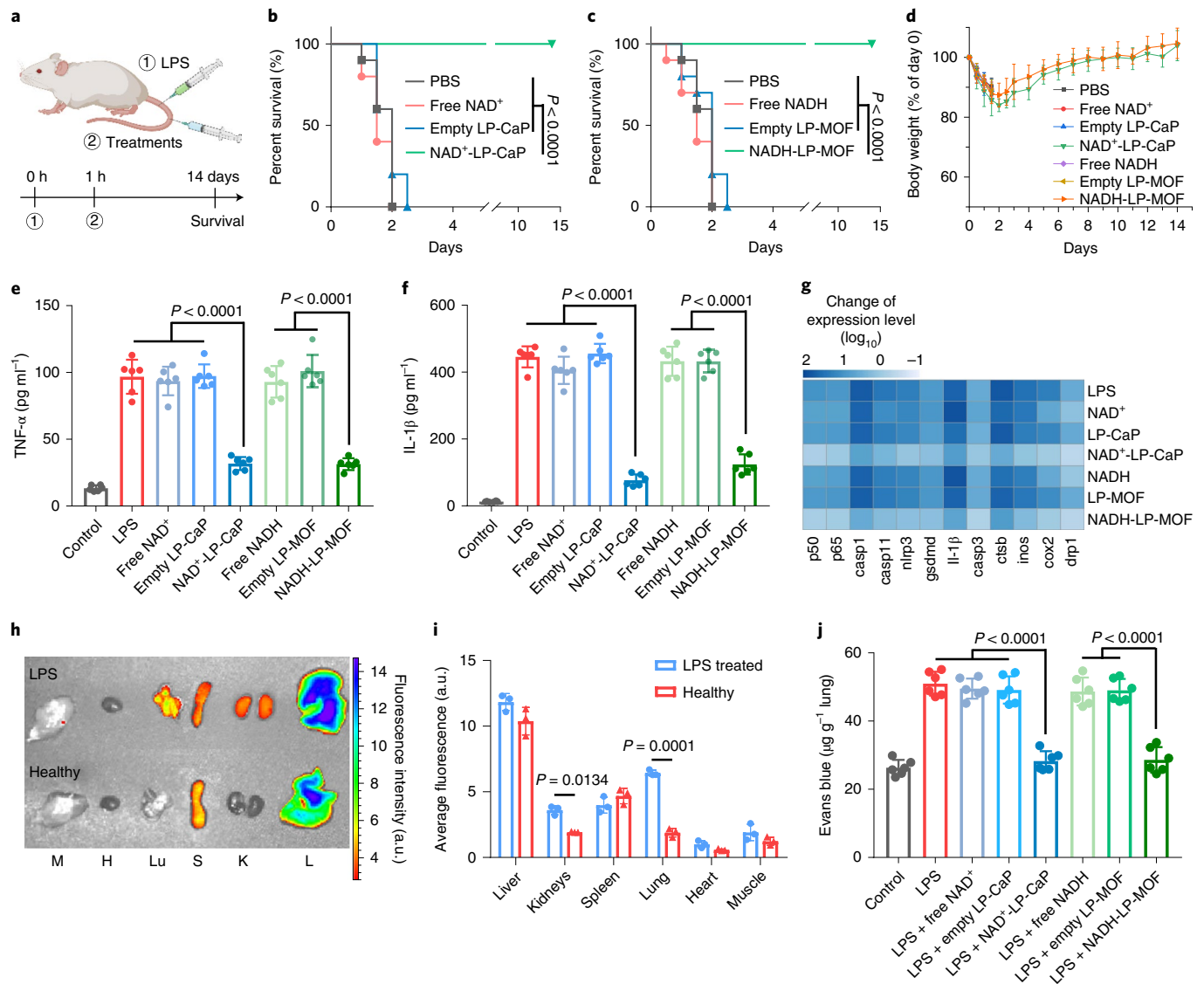
Fig. 3 | The therapeutic efficacy of the NPs in a mouse model of endotoxemia. a, Experimental procedures for the endotoxemia mouse model. Created with BioRender.com. **b–d**, Survival (**b** and **c**) and body weight (**d**) analysis of the mice receiving phosphate-buffered saline (PBS), free NAD(H) (20 mg kg⁻¹) or an equivalent dose of empty NPs and NAD(H)-loaded NPs, with treatment 1 h after LPS (15 mg kg⁻¹) administration. Data are presented as mean ± s.d. (n = 10). Statistical significance was calculated via log-rank test. **e,f**, Pro-inflammatory cytokine TNF-α and IL-1β levels in the serum of septic mice receiving different treatments were measured 6 h after LPS challenge. Data are presented as mean ± s.d. (n = 6). Statistical significance was calculated via one-way ANOVA with Tukey's post hoc test. **g**, Gene expression in the white blood cells of the mice receiving different treatments over negative controls. The colours in the heatmap present the log₁₀ value of relative gene expression. **h**, Ex vivo fluorescence images representing the biodistribution of Cy5.5-labelled LP-CaP NPs in healthy and septic mice 4 h after NP administration. L, K, S, Lu, H and M represent liver, kidneys, spleen, lungs, heart and thigh muscle, respectively. a.u., arbitrary units. **i**, Quantitative analysis of the mean fluorescence intensity of the organ or tissue shown in the ex vivo image. Data are presented as mean ± s.d. (n = 3). Statistical significance was calculated via one-way ANOVA with Tukey's post hoc test. **j**, The vascular hyperpermeability in LPS-stimulated mice receiving different treatments. Evans blue dye was injected 12 h after LPS challenge, and the amount of the dye retained in the lungs was extracted and quantified. Data are presented as mean ± s.d. (n = 6). Statistical significance was calculated via one-way ANOVA with Tukey's post hoc test.

attenuated the ASC speck numbers in BMDMs induced by LPS/ATP, while they nearly blocked the ASC speck formation induced by LPS/lipoLPS, indicating a stronger inhibition to the non-canonical inflammasome pathway (Supplementary Fig. 10). Through inhibition of inflammasome activation, the NAD(H)-loaded NPs also reduced macrophage M1 polarization stimulated by LPS, as indicated by a significantly reduced inducible nitric oxide synthase (iNOS) to arginase-1 (Arg1) expression ratio (Supplementary Fig. 11). As mentioned in previous reports, the regulation of sirtuin activity and the STAT-1/IFN-β pathway are the possible molecular mechanisms of NAD⁺-blocked NF-κB and NLRP3 activation[9,30].

Additionally, the NAD(H)-loaded NPs significantly reduced neutrophil TNF-α production during the inflammation (Supplementary Fig. 12) and blocked NETosis (Supplementary Fig. 13). Since the excessive release of neutrophil extracellular traps (NETs) can induce thrombosis and multiple organ failure, the blockage of NETosis could contribute to decreased vascular dysfunction and multiorgan injury in sepsis.

Inflammation-induced cell apoptosis is a key factor causing multiple organ damage and immune suppression during sepsis[31]. As shown in Fig. 2i,j and Supplementary Fig. 14, the NAD(H)-loaded NPs drastically inhibited cell damage and apoptosis induced by

multiple factors such as inflammation (LPS), oxidative stress (H_2O_2) or NAD$^+$ depletion (FK866). Calcium efflux triggered by endoplasmic reticulum stress and mitochondrial dysfunction induced by NAD$^+$ depletion are the key events that initiate apoptotic signalling. The NAD(H)-loaded NPs that improved cellular NAD$^+$ supply significantly reduced cytosolic calcium concentration (Supplementary Fig. 16) and prevented mitochondrial membrane potential loss (Supplementary Fig. 17), demonstrating their protective effect against apoptosis[32]. In addition to the immune cells, the NAD(H)-loaded NPs also prevented human umbilical vein endothelial cell (HUVEC) apoptosis triggered by TNF-α (Fig. 2k and Supplementary Fig. 15), suggesting that their therapeutic benefit can be applied to many cell types in the context of different inflammatory mediators.

Sepsis-induced endothelial damage and the resultant hypotension is a major cause of mortality[33]. Since the NAD(H)-loaded NPs protected HUVECs from apoptosis, we decided to investigate their ability to inhibit endothelium disruption. Vascular endothelial cadherin (VE-cadherin) is the key protein that forms adherens junctions and maintains vascular integrity[34]. While both LPS and TNF-α disrupted VE-cadherin and destroyed the confluent endothelial monolayer, the NAD(H)-loaded NPs effectively prevented VE-cadherin dissociation and endothelial barrier disruption (Fig. 2l and Supplementary Fig. 18), suggesting their remarkable therapeutic benefit to the vascular system. By contrast, free NAD(H) and the empty NPs did not show much benefit.

Therapeutic efficacy in a mouse model of endotoxemia

The in vivo therapeutic efficacy of the NAD(H)-loaded NPs was tested in a well-established mouse model of LPS-induced endotoxemia (Fig. 3a–d). Mice that received LPS via intravenous (i.v.) administration (15 mg kg^{-1}) all died within three days. Similarly, free NAD(H) and empty NPs demonstrated no amelioration of survival. By contrast, a single injection of either NAD$^+$-LP-CaP or NADH-LP-MOF 1 h after LPS administration was able to rescue 100% of the mice. Although notable body weight loss was initially observed, the mice treated with the NAD(H)-loaded NPs all started to recover after day 3 (Supplementary Fig. 19). A recent bioRχiv paper reported over 85% survival when free NAD$^+$ was used to treat LPS-induced endotoxic shock[9]. However, in their study, free NAD$^+$ was administered two days prior to LPS inoculation, and two injections of extremely high doses (40 mg per mouse per injection, equal to 2,000 mg kg^{-1} per injection for a 20 g mouse) were required, thus making it a prophylactic strategy rather than a therapeutic approach. By contrast, our NAD(H)-loaded NPs given one hour after LPS inoculation required a much lower NAD(H) dose (20 mg kg^{-1}, only one injection) and resulted in 100% survival.

To further evaluate the therapeutic efficacy of the NAD(H)-loaded NPs, cytokine levels in the plasma of LPS-treated mice were tested by enzyme-linked immunosorbent assay (ELISA; Fig. 3e,f). The concentration of pro-inflammatory cytokines TNF-α and IL-1β, the key factors responsible for the cytokine storm and the high mortality in sepsis patients, were drastically reduced after NAD(H)-loaded NP administration. The expression of multiple pro-inflammatory genes was decreased in white blood cells following NAD(H)-loaded NP treatment (Fig. 3g), suggesting an improved immune status in these mice. In addition, the expression of a number of other genes related to cell apoptosis, mitochondrial dysfunction, lysosomal biogenesis and prostanoid release were all downregulated, demonstrating the broad influence of the NAD(H)-loaded NPs on a variety of pathways[35].

The biodistribution of LP-CaP NP and LP-MOF NP was investigated in both healthy mice and LPS-treated mice. Mice were injected (i.v.) with Cy5.5-labelled NPs and killed at 4 h or 24 h post-injection for ex vivo imaging (Fig. 3h,i and Supplementary Figs. 20 and 21). For both NPs, the liver accumulated most of the NPs in both the healthy and LPS-treated mice, while the liver in septic mice cleared the NP much more slowly, possibly due to compromised liver function. In addition to the liver, the septic mice had significantly increased NP distribution in their lungs and kidneys, likely due to endothelial damage and the resultant hyperpermeability. Since liver, lungs and kidneys are more vulnerable to sepsis, leading to severe complications with high morbidity and mortality[36], the preferred NP accumulation in these organs allowed the NAD(H)-loaded NPs to minimize the damage (Supplementary Fig. 23). To support this hypothesis, the ATP levels in all major organs of LPS-treated mice were measured, as energy dysfunction is associated with sepsis-mediated organ failure. While inflammation induced by LPS impaired the energy supply in all major organs, NAD$^+$-LP-CaP effectively recovered the ATP levels (Supplementary Fig. 22), again demonstrating a strong protective effect.

To investigate the NPs' efficacy in ameliorating lung injury and vascular leakage, pulmonary vascular permeability was evaluated by albumin labelled with Evans blue dye (Fig. 3j). The extravasation of Evans blue dye out of the pulmonary vasculature was significantly increased after LPS administration. Compared with free NAD(H) or the empty NP treatments, which did not show any efficacy, the NAD(H)-loaded NPs reduced Evans blue dye leakage to the baseline, suggesting significant efficacy in maintaining pulmonary endothelial function and integrity.

The immune response in sepsis can be characterized by a cytokine-mediated hyperinflammatory phase, and a subsequent immune-suppressive phase[31]. The hyperactive immune system during the first phase may lead to injury of multiple organs; while during the second phase, immunosuppression induced by immune cell apoptosis and dysfunction increases the susceptibility of nosocomial infections[37]. To evaluate the impact of the NAD(H)-loaded NPs on the mouse immune system, immune cell population frequencies and their metabolic status were monitored in LPS-treated mice by flow cytometry (Supplementary Fig. 24). As shown in Fig. 4a,b and Supplementary Fig. 25, the NAD(H)-loaded NPs moderated the neutrophil surge in blood, induced by LPS. The immature/total neutrophil ratio is an indicator of systemic inflammation and the severity of sepsis[38]. While very few neutrophils in healthy mice (3%) were immature neutrophils, the immature/total neutrophil ratio in septic mice increased to 60%, and this number decreased

Fig. 4 | Immune cell population variation, apoptosis and caspase1 activation in the blood, lungs and spleen of endotoxemia mice. a,b, Flow cytometric quantification of monocyte (CD45$^+$CD11b$^+$Ly6C$^+$Ly6G$^-$), neutrophil (CD45$^+$CD11b$^+$Ly6C$^+$Ly6G$^+$), CD4$^+$ T cell (CD45$^+$CD11b^{low}CD3$^+$CD4$^+$) and CD8$^+$ T cell (CD45$^+$CD11b^{low}CD3$^+$CD8$^+$) populations in blood of septic mice 24 h after LPS administration. PBS, free NAD$^+$ (20 mg kg^{-1}) or an equivalent dose of LP-CaP and NAD$^+$-LP-CaP were i.v. injected 1 h after LPS (7.5 mg kg^{-1}, i.v.) administration. Healthy mice without LPS injection were used as the negative control. Data are presented as mean ± s.d. (n = 5). Statistical significance was calculated via one-way ANOVA with Tukey's post hoc test. **c,** Flow cytometric quantification of monocyte and neutrophil populations in the lungs of the septic mice with PBS, free NAD$^+$, LP-CaP or NAD$^+$-LP-CaP treatment. Data are presented as mean ± s.d. (n = 5). Statistical significance was calculated via one-way ANOVA with Tukey's post hoc test. **d,** Representative plots of cell apoptosis for splenic lymphocytes. The grayscale figures on the left show the gating strategy for the CD4$^+$ and CD8$^+$ T cells. **e,f,** Quantification of cell apoptosis (**e**) and caspase1 activation (**f**) for a variety of immune cells (monocyte and neutrophil in blood, and CD4$^+$ and CD8$^+$ T cell in spleen) assessed by annexin V/7AAD staining and FLICA assay, respectively. Data are presented as mean ± s.d. (n = 5). Statistical significance was calculated via one-way ANOVA with Tukey's post hoc test.

to 29% after the treatment of NAD(H)-loaded NPs (Supplementary Fig. 28). In addition to the blood, the NAD(H)-loaded NPs significantly reduced the infiltration of macrophage and neutrophil in the pulmonary alveoli (Fig. 4c and Supplementary Figs. 26 and 27). This finding is in line with the reduced vascular permeability determined by the Evans blue assay, and serves as an indicator of reduced organ

and tissue damage induced by a hyperactive immune response[39]. In addition, the administration of NAD(H)-loaded NPs significantly reduced caspase1 activation in all cell types in the blood and spleen, suggesting the inhibition of cell pyroptosis[40], while free NAD(H) or the empty NPs did not show any observable effect (Fig. 4f and Supplementary Figs. 31 and 32). This finding is consistent with the
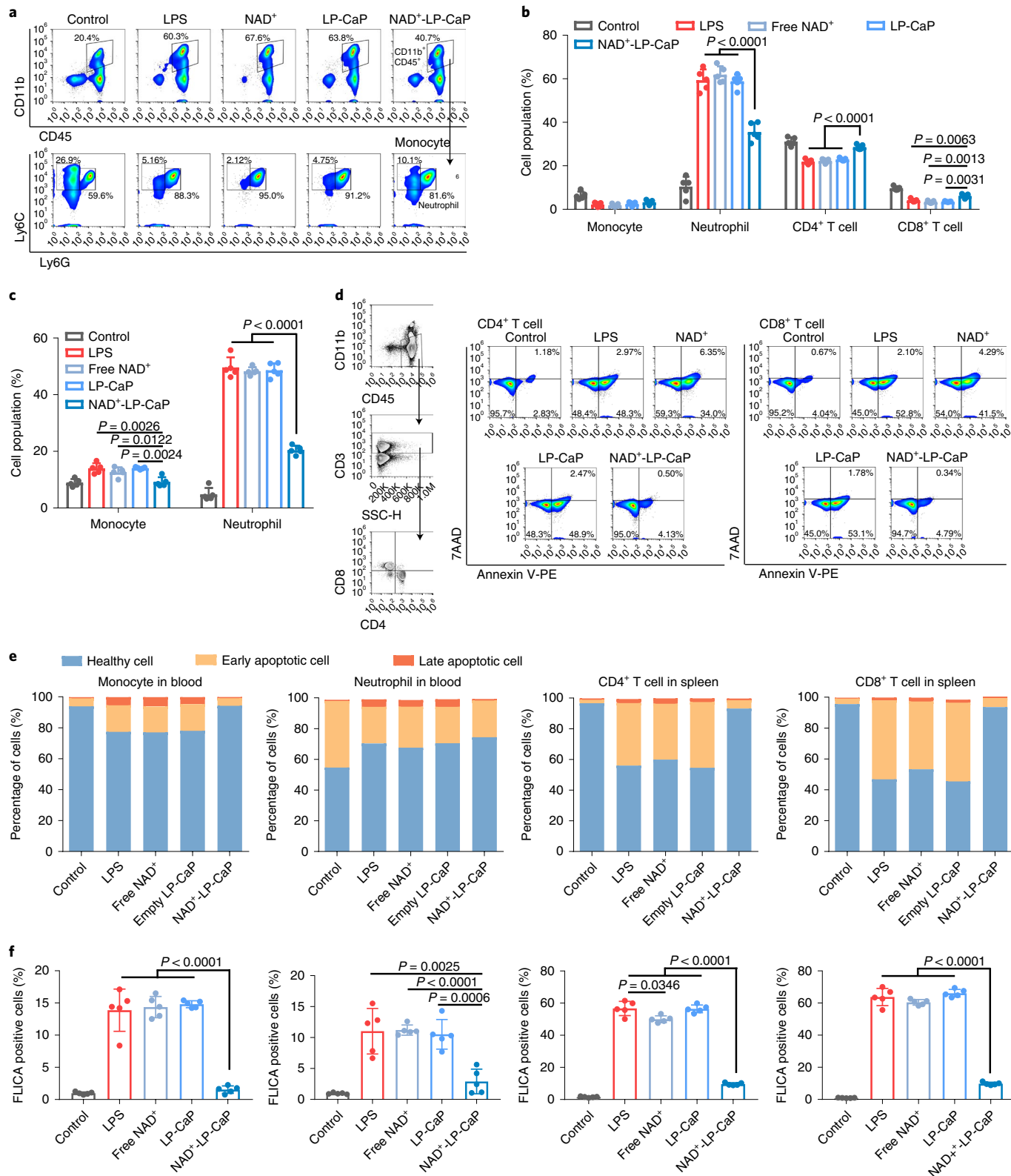
in vitro cell pyroptosis data (Fig. 2c–f and Supplementary Figs. 7 and 8) and in vivo gene expression data obtained by quantitative real-time PCR (qRT-PCR; Fig. 3g). The decreased neutrophil population and caspase1 activation induced by the NAD(H)-loaded NPs demonstrated their high in vivo anti-inflammatory efficacy.

In contrast to pyroptosis, apoptosis is a type of programmed cell death immunologically 'silent' or even anti-inflammatory[41]. Immune cell apoptosis, especially the loss of lymphocytes, is a primary cause of sepsis-induced immunosuppression[37]. The NAD(H)-loaded NPs effectively blocked monocyte and lymphocyte apoptosis in the blood, lungs and spleen of the septic mice, while other treatments did not show observable improvement (Fig. 4d,e and Supplementary Figs. 29 and 30). Notably, lymphocyte apoptosis in spleen—which was more severe than that in blood—was drastically reduced from 50% to the baseline by the NAD(H)-loaded NPs (Fig. 4d). The strong anti-apoptotic effect of the NAD(H)-loaded NPs effectively prevented lymphocyte loss during sepsis (Fig. 4b and Supplementary Figs. 25–27), which is of great significance in maintaining immunity against infections. In contrast to monocytes or lymphocytes, neutrophil apoptosis was much higher under physiological conditions, but it was delayed during sepsis to achieve more efficient killing of invading pathogens[31]. The NAD(H)-loaded NPs did not affect early apoptosis of neutrophils, but they reduced late apoptosis/pyroptosis (Fig. 4e and Supplementary Figs. 29 and 30). The efficient blockage of both pyroptosis and apoptosis demonstrated that the NAD(H)-loaded NPs can be effective immunomodulators to treat sepsis. Since NAD$^+$-LP-CaP and NADH-LP-MOF revealed similar effects for both in vitro and in vivo studies, the NAD$^+$-LP-CaP was chosen as a representative system for the following studies due to its higher payload loading content.

Effect in preventing sepsis-induced persistent injury and immunosuppression

Sepsis patients, surviving the initial cytokine-mediated hyperinflammatory phase, may be prone to infections due to immune suppression and multiorgan injury. In fact, one-third of patients who survive hospitalization for sepsis die during the following year because of complications[42]. Thus, preventing inflammation-induced complications and nosocomial infections are of great significance during sepsis therapy. The immunomodulation effect of NAD$^+$ replenishment and its ability to reduce persistent organ injury were further investigated on a caecal ligation and puncture (CLP)-induced sepsis model with P. aeruginosa secondary infection (Fig. 5a)[43,44]. The CLP infection model mimics human polymicrobial peritoneal infection. CLP infection initiated a hyperinflammatory phase with roughly 30%

mortality at its early stage, which gradually turned to an immunosuppression phase due to the impaired immune system, thus making the animals less resistant to pathogen invasion[45,46]. Free NAD$^+$, empty LP-CaP or NAD$^+$-LP-CaP were i.v. administered twice at 6 h and 24 h, respectively, after the surgery to modulate the inflammation. Three days after CLP, P. aeruginosa was intratracheally inoculated to the mice to mimic the nosocomial infections. While the P. aeruginosa secondary infection was minimally lethal to healthy mice (with 10% mortality in the sham group), it caused a much higher mortality in CLP-treated mice, likely due to a compromised immune system and organ injury (Fig. 5b,c and Supplementary Fig. 33). NAD$^+$-LP-CaP not only mitigated the cytokine storm in the hyperinflammatory stage, leading to a reduction in mortality (from 30% to 7% at day 3), but also prevented CLP-induced multiorgan failure and immunosuppression, as evidenced by the significantly reduced mortality from P. aeruginosa secondary infections (14%, $n = 14$) compared with the untreated group (79%) at day 14. By contrast, free NAD$^+$ and the empty LP-CaP did not improve the survival rate.

Therapeutic efficacy in a polymicrobial blood infection model

Killing pathogens and maintaining a balance of immune homoeostasis are the two primary goals for sepsis therapy. To achieve these two goals simultaneously, rifampicin (Rif), a broad-spectrum antibiotic, was introduced into the LP-CaP NP (denoted as NAD$^+$-Rif-LP-CaP), because we and others demonstrated previously that NPs can improve antibiotic accumulation in infected tissues via the enhanced permeability and retention effect[47]. Rif loaded in the lipid coating layer was released faster than NAD$^+$ encapsulated in the CaP core at pH 7.4 (Supplementary Fig. 34). Thus, the NP can retain most of the NAD$^+$ for intracellular delivery to mammalian cells while also effectively releasing the antibiotic in the infected tissue to kill the bacteria. Since bacteria cannot take up NPs larger than 20 nm (ref. [48]), our NP can specifically deliver NAD$^+$ to mammalian cells rather than bacteria.

The therapeutic efficacy of NAD$^+$-Rif-LP-CaP was evaluated using a polymicrobial blood infection model (Fig. 5d) because sepsis hosts are usually exposed to mixed bacterial infections. A mixture of methicillin-resistant Staphylococcus aureus (MRSA) and P. aeruginosa, two multidrug-resistant pathogens identified as 'serious threats' by the Centers for Disease Control and Prevention, was administered through the tail vein to induce mouse blood infection and sepsis. Different treatments were i.v. administered via a single dose 6 h after the infection. While there was a modest

Fig. 5 | Therapeutic performance of the NAD$^+$-loaded NPs in bacteria-induced sepsis models. a, Experimental procedures for the CLP and P. aeruginosa secondary infection model. Mice subjected to CLP received two i.v. injections of PBS, free NAD$^+$ (20 mg kg^{-1}) or an equivalent dose of LP-CaP and NAD$^+$-LP-CaP at 6 h and 24 h after the surgery and challenged intratracheally with P. aeruginosa (1×10^8 CFU in 50 μl PBS) at day 3. A sham group without CLP and a CLP group without the P. aeruginosa challenge were used as control groups. Created with BioRender.com. **b,c**, Survival (**b**) and body weight (**c**) analysis of the mice in the bacteria secondary infection model. Data are presented as mean ± s.d. ($n = 14$). Statistical significance was calculated via log-rank test. **d**, Experimental procedures for the model of a polymicrobial blood infection induced by MRSA and P. aeruginosa. Mixed multidrug-resistant bacteria (mixed MRSA and P. aeruginosa with 5×10^7 CFU for each pathogen) were i.v. administered to induce blood infection and sepsis, and one injection of different treatments, including PBS, NAD$^+$-LP-CaP, free Rif (acting as a model antibiotic), Rif-LP-CaP or NAD$^+$-Rif-LP-CaP at a dose corresponding to 10 mg Rif per kilogram and 20 mg NAD$^+$ per kilogram were i.v. injected 6 h after the infection. Created with BioRender.com. **e,f**, Survival (**e**) and body weight (**f**) analysis of the mice in the blood infection model. Data are presented as mean ± s.d. ($n = 10$). Statistical significance was calculated via log-rank test. **g**, Bacterial loads in liver, spleen, lungs, kidneys and blood of the septic mice 12 h after the treatments, determined by serial dilution and plate counting. Data are presented as mean ± s.d. ($n = 6$). Statistical significance was calculated via one-way ANOVA with Tukey's post hoc test. Statistical analyses were done relative to the PBS treatment group. **h**, Blood biochemistry analysis demonstrating the liver (alanine transaminase (ALT), aspartate aminotransferase (AST), and alkaline phosphatase (ALP)) and kidney (blood urea nitrogen (BUN)) function of the mice with a bacterial blood infection. Data are presented as mean ± s.d. ($n = 3$). Statistical significance was calculated via one-way ANOVA with Tukey's post hoc test. Statistical analyses were done relative to the PBS treatment group. **i**, Representative histological images for tissue sections with haematoxylin and eosin staining and terminal deoxynucleotidyl transferase dUTP nick end labeling (TUNEL) staining, from the healthy mice (control) and the infected mice with PBS or NAD$^+$-Rif-LP-CaP treatments. OSOM, outer stripe of outer medulla; ISOM, inner stripe of outer medulla. Representative images of three independent experiments. Scale bar, 100 μm.

survival benefit following treatment with NAD$^+$-LP-CaP, free Rif and Rif-LP-CaP (Fig. 5e,f and Supplementary Fig. 35), treatment with NAD$^+$-Rif-LP-CaP with both antimicrobial and immunomodulation capabilities resulted in 90% mouse survival after two weeks, demonstrating an excellent therapeutic outcome.

The bacterial colony forming units (CFUs) in mouse blood and different organs were measured 12 h after bacterial infection (Fig. 5g). While free Rif or Rif-loaded NPs reduced the bacterial burden in most of the organs, NAD$^+$-LP-CaP did not affect bacterial clearance. Additionally, mice treated with Rif-loaded NPs (that is, Rif-LP-CaP or NAD$^+$-Rif-LP-CaP) had significantly lower CFUs in the liver and lungs compared with those treated with free Rif. These findings can be attributed to the elevated NP accumulation in these organs (Fig. 3h,i and Supplementary Fig. 20).

The therapeutic efficacy of NAD$^+$-Rif-LP-CaP in preventing multiple organ failure, the hallmark of sepsis responsible for high
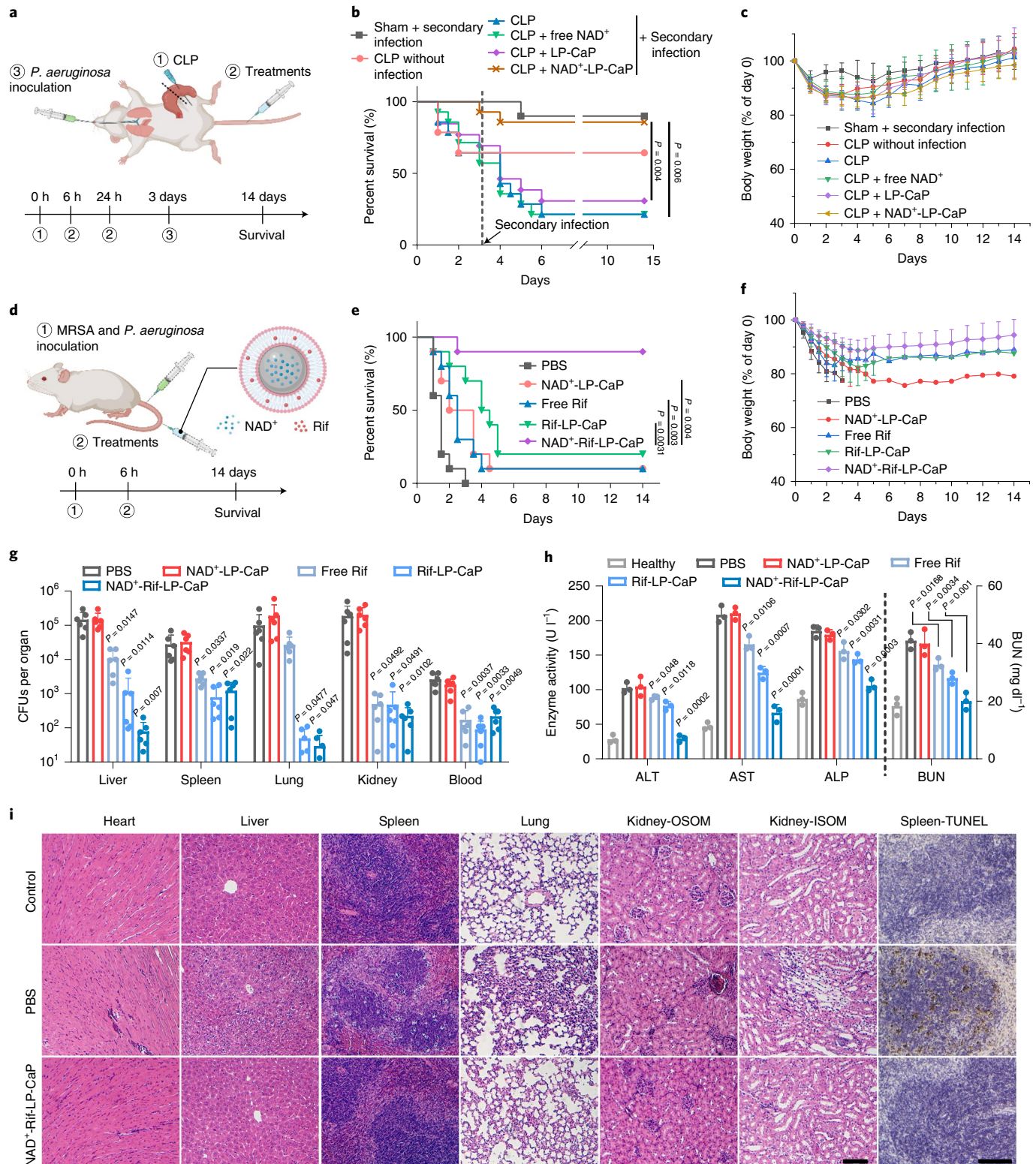
mortality, was evaluated by blood biochemical analysis. While the serum biomarkers for liver and kidney injuries were significantly elevated after bacterial inoculation, NAD^{+}-Rif-LP-CaP effectively protected the organs from infection-induced damage and reduced the biochemical parameters to near baseline (Fig. 5h and Supplementary Fig. 37). By contrast, free Rif and Rif-LP-CaP slightly mitigated the injury, while NAD^{+}-LP-CaP, unable to inhibit bacterial growth, did not demonstrate any benefit. Histopathological analysis (Fig. 5i and Supplementary Fig. 36) was further used to substantiate the therapeutic benefit indicated by the biochemical data. In the septic mice, sections stained with haematoxylin and eosin revealed typical multiple organ injury. NAD^{+}-Rif-LP-CaP significantly reduced multiple organ injury, while other treatments demonstrated little efficacy. Healthy mice subjected to three administrations of the NPs every other day did not show any significant organ damage, monitored by tissue histological analysis, demonstrating the desirable biosafety of these NPs (Supplementary Fig. 38).

Conclusions

In summary, we engineered a family of NAD(H)-loaded NPs capable of direct and efficient intracellular NAD(H) delivery suitable for in vivo therapeutic studies. The NAD(H)-loaded NPs improved cellular energy supply, suppressed inflammation, prevented inflammation-induced cell apoptosis and pyroptosis and helped maintain immune homoeostasis and vascular function, two key factors in the pathogenesis of sepsis. This family of NAD(H)-loaded NPs demonstrated excellent therapeutic efficacy in treating multidrug-resistant pathogen-induced polymicrobial bacteremia, preventing secondary infections and ameliorating multiple organ injury, while exhibiting good biocompatibility. Therefore, this study may pave the road for the development of a highly innovative and translational approach for sepsis. In addition to sepsis, the NAD(H)-loaded NPs as effective immunomodulators could potentially be applied in other inflammation-related scenarios, such as COVID-19 treatment or organ grafting.

Online content

Any methods, additional references, Nature Research reporting summaries, source data, extended data, supplementary information, acknowledgements, peer review information; details of author contributions and competing interests; and statements of data and code availability are available at https://doi.org/10.1038/s41565-022-01137-w.

References

1. Rudd, K. E. et al. Global, regional, and national sepsis incidence and mortality, 1990–2017: analysis for the Global Burden of Disease Study. *Lancet* **395**, 200–211 (2020).
2. Dugar, S., Choudhary, C. & Duggal, A. Sepsis and septic shock: guideline-based management. *Clevel. Clin. J. Med.* **87**, 53–64 (2020).
3. Rhodes, A. et al. Surviving sepsis campaign: international guidelines for management of sepsis and septic shock: 2016. *Intensive Care Med.* **43**, 304–377 (2017).
4. Grahnert, A. et al. NAD+: a modulator of immune functions. *Innate Immun.* **17**, 212–233 (2011).
5. Hong, G. et al. Administration of nicotinamide riboside prevents oxidative stress and organ injury in sepsis. *Free Radic. Biol. Med.* **123**, 125–137 (2018).
6. Nadlinger, K., Birkmayer, J., Gebauer, F. & Kunze, R. Influence of reduced nicotinamide adenine dinucleotide on the production of interleukin-6 by peripheral human blood leukocytes. *Neuroimmunomodulation* **9**, 203–208 (2001).
7. Van Gool, F. et al. Intracellular NAD levels regulate tumor necrosis factor protein synthesis in a sirtuin-dependent manner. *Nat. Med.* **15**, 206–210 (2009).
8. Gerner, R. R. et al. NAD metabolism fuels human and mouse intestinal inflammation. *Gut* **67**, 1813–1823 (2018).
9. Iske, J. et al. NAD^{+} prevents septic shock by non-canonical inflammasome blockade and IL-10. Preprint at *bioRxiv* https://doi.org/10.1101/2020.03.29.013649 (2020).
10. Biefer, H. R. C. et al. Mast cells regulate CD4^{+} T-cell differentiation in the absence of antigen presentation. *J. Allergy Clin. Immunol.* **142**, 1894–1908.E7 (2018).
11. Dongsheng, W., Sili, Z., Minghe, C. & Chaoyu, M. Effect of nicotinamide mononucleotide on mortality of mice with endotoxic shock. *J. Pharm. Pract.* **39**, 134–137 (2021).
12. Cantó, C., Menzies, K. J. & Auwerx, J. NAD[+] metabolism and the control of energy homeostasis: a balancing act between mitochondria and the nucleus. *Cell Metab.* **22**, 31–53 (2015).
13. Ratajczak, J. et al. NRK1 controls nicotinamide mononucleotide and nicotinamide riboside metabolism in mammalian cells. *Nat. Commun.* **7**, 13103 (2016).
14. Chong, Z.-Z., Lin, S.-H., Li, F. & Maiese, K. The sirtuin inhibitor nicotinamide enhances neuronal cell survival during acute anoxic injury through AKT, BAD, PARP, and mitochondrial associated. *Curr. Neurovascular Res.* **2**, 271–285 (2005).
15. Klaidman, L. et al. Nicotinamide offers multiple protective mechanisms in stroke as a precursor for NAD^{+}, as a PARP inhibitor and by partial restoration of mitochondrial function. *Pharmacology* **69**, 150–157 (2003).
16. Chen, H. et al. NAD^{+}-carrying mesoporous silica nanoparticles can prevent oxidative stress-induced energy failures of both rodent astrocytes and PC12 cells. *PLoS One* **8**, e74100 (2013).
17. Han, Y. Y. et al. Liposomal ATP or NAD^{+} protects human endothelial cells from energy failure in a cell culture model of sepsis. *Res. Commun. Mol. Pathol. Pharmacol.* **110**, 107–116 (2001).
18. Remick, D. G. Pathophysiology of sepsis. *Am. J. Pathol.* **170**, 1435–1444 (2007).
19. Crowley, C., Payne, C., Bernstein, H., Bernstein, C. & Roe, D. The NAD^{+} precursors, nicotinic acid and nicotinamide protect cells against apoptosis induced by a multiple stress inducer, deoxycholate. *Cell Death Differ.* **7**, 314–326 (2000).
20. Li, J., Yang, Y. & Huang, L. Calcium phosphate nanoparticles with an asymmetric lipid bilayer coating for siRNA delivery to the tumor. *J. Controlled Release* **158**, 108–114 (2012).
21. Li, J., Chen, Y.-C., Tseng, Y.-C., Mozumdar, S. & Huang, L. Biodegradable calcium phosphate nanoparticle with lipid coating for systemic siRNA delivery. *J. Controlled Release* **142**, 416–421 (2010).
22. Yang, H. et al. Nutrient-sensitive mitochondrial NAD^{+} levels dictate cell survival. *Cell* **130**, 1095–1107 (2007).
23. Zapata-Pérez, R., Wanders, R. J., van Karnebeek, C. D. & Houtkooper, R. H. NAD[+] homeostasis in human health and disease. *EMBO Mol. Med.* **13**, e13943 (2021).
24. Cameron, A. M. et al. Inflammatory macrophage dependence on NAD^{+} salvage is a consequence of reactive oxygen species–mediated DNA damage. *Nat. Immunol.* **20**, 420–432 (2019).
25. Weiss, R. et al. Nicotinamide: a vitamin able to shift macrophage differentiation toward macrophages with restricted inflammatory features. *Innate Immun.* **21**, 813–826 (2015).
26. Henry, B. D. et al. Engineered liposomes sequester bacterial exotoxins and protect from severe invasive infections in mice. *Nat. Biotechnol.* **33**, 81–88 (2015).
27. Martínez-García, J. J. et al. P2X7 receptor induces mitochondrial failure in monocytes and compromises NLRP3 inflammasome activation during sepsis. *Nat. Commun.* **10**, 2711 (2019).
28. Hagar, J. A., Powell, D. A., Aachoui, Y., Ernst, R. K. & Miao, E. A. Cytoplasmic LPS activates caspase-11: implications in TLR4-independent endotoxic shock. *Science* **341**, 1250–1253 (2013).
29. Kayagaki, N. et al. Caspase-11 cleaves gasdermin D for non-canonical inflammasome signalling. *Nature* **526**, 666–671 (2015).
30. Dempsey, L. A. Sirtuin regulation of NLRP3. *Nat. Immunol.* **21**, 358–358 (2020).
31. Hotchkiss, R. S., Monneret, G. & Payen, D. Sepsis-induced immunosuppression: from cellular dysfunctions to immunotherapy. *Nat. Rev. Immunol.* **13**, 862–874 (2013).
32. Wendel, M. & Heller, A. R. Mitochondrial function and dysfunction in sepsis. *Wien. Medizinische Wochenschr.* **160**, 118–123 (2010).
33. Lupu, F., Kinasewitz, G. & Dormer, K. The role of endothelial shear stress on haemodynamics, inflammation, coagulation and glycocalyx during sepsis. *J. Cell. Mol. Med.* **24**, 12258–12271 (2020).
34. Polacheck, W. J. et al. A non-canonical Notch complex regulates adherens junctions and vascular barrier function. *Nature* **552**, 258–262 (2017).
35. Szekanecz, Z., Szamosi, S., Kovács, G. E., Kocsis, E. & Benkő, S. The NLRP3 inflammasome-interleukin 1 pathway as a therapeutic target in gout. *Arch. Biochem. Biophys.* **670**, 82–93 (2019).
36. Caraballo, C. & Jaimes, F. Organ dysfunction in sepsis: an ominous trajectory from infection to death. *Yale J. Biol. Med.* **92**, 629–640 (2019).

37. Venet, F. & Monneret, G. Advances in the understanding and treatment of sepsis-induced immunosuppression. *Nat. Rev. Nephrol.* **14**, 121–137 (2018).

38. Darnifayanti, D., Tjipta, G. D., Rusdidjas, R. & Lubis, B. M. Immature-to-total neutrophil ratio as an early diagnostic tool of bacterial neonatal sepsis. *Paediatr. Indones.* **55**, 153–157 (2015).

39. Zhu, Y. G. et al. Human mesenchymal stem cell microvesicles for treatment of *Escherichia coli* endotoxin- induced acute lung injury in mice. *Stem Cells* **32**, 116–125 (2014).

40. Ataide, M. A. et al. Malaria-induced NLRP12/NLRP3-dependent caspase-1 activation mediates inflammation and hypersensitivity to bacterial superinfection. *PLoS Pathog.* **10**, e1003885 (2014).

41. Arienti, S., Barth, N. D., Dorward, D. A., Rossi, A. G. & Dransfield, I. Regulation of apoptotic cell clearance during resolution of inflammation. *Front. Pharmacol.* https://doi.org/10.3389/fphar.2019.00891 (2019).

42. Prescott, H. C. & Angus, D. C. Enhancing recovery from sepsis: a review. *JAMA* **319**, 62–75 (2018).

43. Shang, S. et al. Artesunate interacts with the vitamin D receptor to reverse sepsis-induced immunosuppression in a mouse model via enhancing autophagy. *Br. J. Pharmacol.* **177**, 4147–4165 (2020).

44. Nascimento, D. C. et al. Role of regulatory T cells in long-term immune dysfunction associated with severe sepsis. *Crit. Care Med.* **38**, 1718–1725 (2010).

45. Grailer, J. J., Kalbitz, M., Zetoune, F. S. & Ward, P. A. Persistent neutrophil dysfunction and suppression of acute lung injury in mice following cecal ligation and puncture sepsis. *J. Innate Immun.* **6**, 695–705 (2014).

46. Pugh, A. M., Auteri, N. J., Goetzman, H. S., Caldwell, C. C. & Nomellini, V. A murine model of persistent inflammation, immune suppression, and catabolism syndrome. *Int. J. Mol. Sci.* **18**, 1741 (2017).

47. Ye, M. et al. A dual-responsive antibiotic-loaded nanoparticle specifically binds pathogens and overcomes antimicrobial-resistant infections. *Adv. Mater.* **33**, 2006772 (2021).

48. Butler, K. S., Peeler, D. J., Casey, B. J., Dair, B. J. & Elespuru, R. K. Silver nanoparticles: correlating nanoparticle size and cellular uptake with genotoxicity. *Mutagenesis* **30**, 577–591 (2015).

Methods

Materials. β-nicotinamide adenine dinucleotide (NAD⁺), reduced β-nicotinamide adenine dinucleotide (NADH), calcium chloride ($CaCl_2$), disodium hydrogen phosphate (Na_2HPO_4), zinc nitrate hexahydrate, 2-methylimidazole and LPS (from *Escherichia coli* O111:B4) were purchased from Sigma-Aldrich. Soy PC and DOPA were purchased from Avanti Polar Lipids. Other reagents and solvents were purchased from Thermo Fisher Scientific and used as received unless otherwise stated.

NAD⁺-LP-CaP formulation. NAD⁺-LP-CaP was prepared via a water-in-oil reverse microemulsion method followed by thin-film hydration[20]. Briefly, two water-in-oil reverse microemulsions (25 ml) dispersed in a cyclohexane/IGEPAL CO-520 (71:29, v/v) oil phase were prepared. Emulsion 1 contained 500 μl $CaCl_2$ solution (2.5 M) with 1 mg NAD⁺, while emulsion 2 contained 500 μl Na_2HPO_4 solution (25 mM, pH 9) with 3 mg DOPA. The two emulsions were mixed and stirred for 30 min. Ethanol (50 ml) was added to remove the oil phase, and the NP was pelleted by centrifugation at 10,000g for 20 min. After being extensively washed by ethanol three times, the NP together with Soy PC (3 mg) and cholesterol (0.3 mg) was dissolved in chloroform. After the chloroform was removed by a rotary evaporator, the lipid film was then rehydrated in 500 μl Tris-HCl buffer (10 mM, pH 7.4) to obtain NAD⁺-LP-CaP. NAD⁺ and Rif coloaded nanoparticles (NAD⁺-Rif-LP-CaP) with Rif encapsulated in the lipid coating layer were prepared with the aforementioned processes by adding Rif together with Soy PC and cholesterol.

NADH-LP-MOF formulation. NADH (6.6 mg) and zinc nitrate hexahydrate (18.6 mg) were dissolved in 35 ml deionized water. Then 2-methylimidazole (166 mg, dissolved in 10 ml deionized water) was added to the NADH solution. The resultant mixture was vortexed for 10 s and then kept still for 5 min to allow MOF growth. The MOF NP was then pelleted through centrifugation at 10,000g for 45 min, redispersed in 1.5 ml water and ultrasonicated 30 times. The MOF NPs were mixed with a liposome solution (composed of Soy PC and cholesterol, 10:1 w/w, 40 mg ml⁻¹) and extruded through a 0.4 μm polycarbonate porous membrane using an Avanti mini-extruder to obtain NADH-LP-MOF.

Characterization. The hydrodynamic size and zeta potential of the NPs were measured by dynamic light scattering (ZetaSizer Nano ZS90, Malvern Instruments) at a concentration of 0.1 mg ml⁻¹. The morphologies of the NPs were visualized by transmission electron microscopy (Philips CM200 Ultra Twin) with phosphotungstic acid staining. To evaluate the drug loading efficiency and loading content of the NAD(H)-loaded NPs, the NPs were dissolved in 0.01 M HCl to release NAD(H). The pH of the solutions was adjusted to neutral, and the NAD(H) concentration was determined using an Amplite Colorimetric Total NAD and NADH Assay Kit (AAT Bioquest).

In vitro release kinetics of NAD(H) and Rif from the NPs under different pH conditions were studied by a dialysis method. The NPs (3 ml, containing 6 mg NAD(H) or 3 mg Rif) were sealed in dialysis bags (molecular weight cut-off of 3,500 Da) and immersed in 40 ml buffer with different pH values (pH 5.5, 6.5, 7.4). The dialysis systems were incubated in a 37 °C shaker, and 100 μl samples outside the dialysis bag were collected at different time intervals for NAD(H) quantification. An equal volume of prewarmed fresh medium was added back to the release medium.

Cell culture. BMDMs were isolated and cultured as described previously[49]. Mouse neutrophils were isolated by Percoll-based density gradient centrifugation and used fresh[50]. HUVECs (PCS-100-013, ATCC) were cultured in endothelial basal medium (ATCC) supplemented with endothelial cell growth kit VEGF (ATCC) at 37 °C in 5% CO_2 atmosphere. The passage number of HUVECs used in this study was between 4 and 7. Murine macrophage cell line RAW 264.7 (TIB-71, ATCC) and human embryonic kidney cell line HEK 293 (CRL-3216, ATCC) were maintained in RPMI-1640 (Gibco) and DMEM media, respectively.

Cellular NAD(H) level. BMDMs were seeded into a 96-well plate (7×10^4 cells per well) and cultured overnight. Thereafter, the cells were treated with 10 μM free NAD(H) or NAD(H)-loaded NPs with an equivalent amount of NAD(H) (10 μM) and incubated with LPS (100 ng ml⁻¹), H_2O_2 (0.5 mM) or FK866 (20 nM) for 12 h. Subsequently, the cells were washed with PBS three times and lysed using 50 μl lysis buffer. The cellular NAD(H) level was assessed using the Total NAD and NADH Assay Kit. To further evaluate the NAD⁺/NADH ratio after different treatments, BMDMs were seeded in a 24-well plate (1×10^6 cells per well) and cultured overnight. Subsequently, the cells were subjected to various treatment conditions as stated above for 12 h, and then lysed. The NAD⁺/NADH ratio was measured by an Amplite Colorimetric NAD/NADH Ratio Assay Kit (catalog no. 15273, AAT Bioquest) according to the manufacturer's instructions.

Cell viability and ATP-level assays. BMDMs were seeded into a 96-well plate (2×10^4 cells per well) and cultured overnight. Subsequently, cells were treated with free NAD(H), empty NPs or NAD(H)-loaded NPs, together with LPS (100 ng ml⁻¹) or NAD⁺ synthesis inhibitor (FK866, 20 nM) for 48 h, or H_2O_2

(0.5 mM) for 12 h. Cell viability was measured using a standard MTT assay, and cellular ATP levels were tested using a luminescent ATP detection kit (catalog no. ab65348, Abcam). Data were collected using a GloMax-Multi Microplate Multimode Reader (Promega).

Cell pyroptosis assays. BMDMs were cultured overnight in a 96-well plate (2×10^4 cells per well) and primed with LPS (100 ng ml⁻¹) for 3 h as the signal 1 of the NLRP3 inflammasome pathway. The cells were then stimulated with either ATP (2.5 mM, signal 2 for the canonical inflammasome pathway) for another 1 h, or lipoLPS (100 ng LPS per well, signal 2 for the non-canonical inflammasome pathway) in serum-free media for 3 h (refs. [28,29]). Cells were incubated with different treatments (free NAD(H), empty NPs and NAD(H)-loaded NPs with an equivalent NAD(H) dose of 10 μM) together with either signal 1, signal 2 or both. Twelve hours after the treatment, cells were stained with FAM–FLICA probe 5-FAM-YVAD-FMK (catalog no. 13473, AAT Bioquest) to monitor caspase1 activation. The IL-1β and lactate dehydrogenase release in the cell culture medium were tested by ELISA (R&D Systems) and lactate dehydrogenase assay kit (catalog no. 786-210, GBiosciences), respectively. All the assays above were performed according to the manufacturer's protocol.

Measurement of inflammation-related cytokine levels. BMDMs were seeded into a 96-well plate (2×10^4 cells per well) and treated with LPS (100 ng ml⁻¹) together with free NAD(H), empty NPs or NAD(H)-loaded NPs with an equivalent NAD(H) dose of 10 μM. Twelve hours after the treatment, the cell culture media were collected to analyse the cytokine production by ELISA kits supplied by R&D Systems according to the manufacturer's instructions. Data were collected by monitoring the difference between the absorbance at 450 nm and 570 nm using the Microplate Reader.

ASC speck formation. BMDMs seeded into confocal dishes (3×10^5 cells per dish) overnight were primed with LPS (100 ng ml⁻¹, 3 h) and then stimulated with either ATP (2.5 mM) for 1 h or lipoLPS (1 μg LPS per dish, in serum-free media) for 3 h. Different treatments, including free NAD(H), empty NPs and NAD(H)-loaded NPs with an equivalent NAD(H) dose of 10 μM, were given together with the stimuli. The cells were fixed with freshly prepared 4% paraformaldehyde PBS solution for 20 min at room temperature and then permeabilized with 0.5% Triton X-100 for 15 min. After the cells were blocked with 10% normal goat serum at room temperature for 1 h, they were incubated with Alexa Fluor 488-labelled anti-ASC antibody (Santa Cruz) for 2 h, and then stained with DAPI for 15 min at room temperature. ASC speck was then observed by CLSM.

NF-κB p65 nuclear translocation. BMDMs seeded in confocal dishes (3×10^5 cells per dish) overnight were pretreated with free NAD(H), empty NPs or NAD(H)-loaded NPs (with an equivalent NAD(H) dose of 10 μM) for 5 h, and then stimulated with LPS (100 ng ml⁻¹) for 1 h. The cells were fixed with freshly prepared 4% paraformaldehyde PBS solution for 20 min at room temperature and then permeabilized with 0.5% Triton X-100 for 15 min. After the cells were blocked with 10% normal goat serum for 1 h at room temperature, they were incubated with Alexa Fluor 488-labelled anti-NF-κB p65 antibody (F-6, Santa Cruz) for 2 h, and then stained with DAPI for 15 min at room temperature. The p65 nuclear translocation was observed by CLSM.

Apoptosis analysis. BMDMs or HUVECs were seeded into 96-well plates (2×10^4 cells per well) and cultured overnight. BMDMs were then incubated with LPS (100 ng ml⁻¹) or FK866 (20 nM) for 48 h, or H_2O_2 (0.5 mM) for 12 h. HUVECs were incubated with LPS (100 ng ml⁻¹), FK866 (20 nM) or TNF-α (80 ng ml⁻¹) for 48 h. Different treatments, including free NAD(H), empty NPs and NAD(H)-loaded NPs (with an equivalent NAD(H) dose of 10 μM), were added together with the stimuli. Thereafter, the cells were stained with annexin V and propidium iodide (BD Biosciences) in the annexin V binding solution at room temperature for 20 min. Apoptotic cells were quantified using flow cytometry. The data were analysed using FlowJo software (Tree Star).

Quantification of intracellular calcium levels. BMDMs with or without LPS (100 ng ml⁻¹) stimulation were incubated with free NAD(H) (10 μM), empty NPs or NAD(H)-loaded NPs with an equivalent NAD(H) dose of 10 μM for 8 h. The cells were then stained with Fluo-3/AM (2 μM, catalog no. S1056, Beyotime) for 0.5 h and monitored by flow cytometry.

Visualization of tight junctions. HUVEC monolayers were treated with free NAD(H), empty NPs or NAD(H)-loaded NPs, together with LPS (4 μg ml⁻¹) or TNF-α (100 ng ml⁻¹) for 24 h. The cells were fixed with 4% paraformaldehyde PBS solution and permeabilized with 0.5% Triton X-100. After the cells were blocked with 10% normal goat serum for 1 h, they were incubated with Alexa Fluor 488-labelled VE-cadherin antibody (Santa Cruz) for 2 h, stained with DAPI for 15 min at room temperature and then observed by CLSM.

Mitochondrial membrane potentials assay. A JC-1 fluorescence probe was used to evaluate the mitochondrial depolarization in BMDMs. Briefly, cells cultured in

confocal dishes were treated with free NAD(H), empty NPs and NAD(H)-loaded NPs, and incubated with LPS (100 ng ml^{-1}) or FK866 (20 nM) for 24 h, or H$_2$O$_2$ (0.5 mM) for 6 h. Then, the cell medium was discarded, and serum-free medium containing the JC-1 probe (5 μg ml^{-1}, catalog no. AG-CR1-3568, AdipoGen Life Sciences) was added. The cells were incubated at 37 °C for 30 min. Subsequently, cells were stained with DAPI and observed by CLSM.

qRT-PCR analysis. BMDMs were seeded in 24-well plates (2×10^5 cells per well) and allowed to grow for 12 h. Then, cells were primed with LPS (100 ng ml^{-1}, 3 h) and stimulated with either ATP (2.5 mM) for 1 h or lipoLPS (0.5 μg LPS per well, in serum-free media) for 3 h. Free NAD(H), empty NPs or NAD(H)-loaded NPs with an equivalent NAD(H) dose of 10 μM were incubated together with the stimuli. Total cell RNA was extracted using TRIzol reagent (Invitrogen) according to the manufacturer's instructions. RNA was converted to cDNAs by an iScript Reverse Transcription Supermix for qRT-PCR (BIO-RAD). qRT-PCR was performed with an iTaq Universal SYBR Green Supermix (BIO-RAD)[51]. The primers used for qRT-PCR are listed in Supplementary Table 1.

Animals and ethics. All animal experiments were performed under the Guide for the Care and Use of Laboratory Animals (National Institutes of Health) and protocol (M006127) approved by the Institutional Animal Care and Use Committee (IACUC) at the University of Wisconsin. BALB/c (female, 8–12 weeks, The Jackson Laboratory) mice were used for the in vivo experiments.

In vivo biodistribution study. Mice were intravenously injected with LPS (7.5 mg kg^{-1}) to induce endotoxemia. Twelve hours later, Cy5.5-loaded LP-CaP or LP-MOF (0.5 mg kg^{-1}) was injected to the endotoxemia or healthy mice via tail vein. Mice (n = 3) were killed 4 h and 24 h after NP injection. Major organs were collected for IVIS analysis with an excitation band-pass filter at 676 nm and emission at 705 nm. For the evaluation of ATP levels in different organs, mice were challenged with LPS (15 mg kg^{-1}, i.v.) and treated with free NAD$^+$ (20 mg kg^{-1}), or an equivalent dose of LP-CaP and NAD$^+$-LP-CaP (20 mg kg^{-1} of NAD$^+$) after 1 h. The mice were killed 24 h after LPS administration, and different organs or tissues were collected, weighed, homogenized and lysed for ATP quantification using a luminescent ATP detection kit (catalog no. S0026, Beyotime).

Survival study in the mouse model of endotoxemia. Mice were intravenously injected with LPS (15 mg kg^{-1}) through the tail vein. After one hour, mice were grouped randomly and intravenously injected with various formulations including PBS, free NAD$^+$, empty LP-CaP, NAD$^+$-LP-CaP, free NADH, empty LP-MOF and NADH-LP-MOF (with an equivalent NAD(H) dose of 20 mg kg^{-1}). Mice were monitored for their behavioural profile over the duration of the experiments according to the animal protocol guidelines. The survival and body weight of the mice were recorded over time and presented using Kaplan–Meier curves (n = 10).

Quantification of pro-inflammatory cytokine and inflammation-related gene expression in the mouse model of endotoxemia. LPS (7.5 mg kg^{-1}) was injected through the tail vein to induce endotoxemia. One hour after the LPS injection, LPS-induced endotoxemia mice were intravenously treated with PBS, free NAD(H), empty NPs and NAD(H)-loaded NPs with an equivalent NAD(H) dose of 20 mg kg^{-1}. Six hours after the LPS challenge, blood was collected from the orbital sinus and centrifuged at 300g for 10 min to separate blood cells and plasma. The pro-inflammatory cytokine levels (TNF-α and IL-1β) in the plasma were determined by ELISA kits. The white blood cells were collected for qRT-PCR analysis (n = 6).

Lung vascular permeability measurements. LPS-induced endotoxemia mice (7.5 mg kg^{-1}, i.v.) were intravenously treated with PBS, free NAD(H), empty NPs and NAD(H)-loaded NPs with an equivalent NAD(H) dose of 20 mg kg^{-1} 1 h after LPS inoculation. Twelve hours after the LPS challenge, 150 μl Evans blue and albumin (1% Evans blue dye and 4% albumin in PBS) was i.v. injected and allowed to circulate in the blood vessels for 1 h. Mice were scarified and lung tissues were collected and homogenized in 1 ml PBS. Evans blue was then extracted in 2 ml formamide, at 60 °C overnight. Evans blue concentration in the lung homogenate supernatants was quantified by the spectrophotometric method at absorbances of 620 nm and 740 nm to determine the dye leakage (n = 6)[26].

Flow cytometry. LPS-induced endotoxemia mice (7.5 mg kg^{-1}, i.v.) were intravenously treated with PBS, free NAD(H), empty NPs and NAD(H)-loaded NPs with an equivalent NAD(H) dose of 20 mg kg^{-1} at 1 h after LPS inoculation. Twenty-four hours after the LPS challenge, mice were killed, and their blood, lungs and spleen were collected (n = 5). Immune cells in the lungs and spleen were isolated by squeezing through a 70 μm nylon mesh to create the single cell suspension. Red blood cells were lysed using ACK buffer (BioWhittaker) and cells were washed with PBS twice. The isolated cells were blocked with anti-mouse CD16/CD32 antibody (eBioscience) for 15 min and stained with FLICA or apoptosis antibody panels (Supplementary Table 2). Flow cytometry was performed on an Attune NxT cytometer using standard procedures. Gating strategies were set based on fluorescence minus one samples.

CLP and *P. aeruginosa* secondary infection model. Mice were anaesthetized with isoflurane. Thereafter, the abdominal cavity was opened with a midline incision to expose the caecum. The distal 50% of the caecum was ligated with a 6-0 silk suture and perforated with a 19-gauge needle twice. Subsequently, a small amount of faeces was squeezed out and spread around the caecum. The caecum was relocated into the peritoneal cavity, and the laparotomy site was closed, followed by subcutaneous injection of 1 ml resuscitative prewarmed sterile saline[52]. This level of injury was utilized to create a prolonged infection that impaired the immune system and induced an approximate 30% mortality. Two injections of PBS, free NAD$^+$ (20 mg kg^{-1} per injection), LP-CaP or NAD$^+$-LP-CaP (an equivalent dose of NAD$^+$ of 20 mg kg^{-1} per injection) were given through the tail vein 6 h and 24 h after the surgery. At day 3 post CLP, the surviving mice were anaesthetized and infected with *P. aeruginosa* (ATCC 27853, 1×10^8 CFU in 50 μl PBS solution) through intratracheal injection, to mimic nosocomial infections. A rodent intubation stand with 45° angle and a syringe fitted with a polyethylene tubing PE-10 were used for the intratracheal instillation. After anaesthesia, the mice were suspended by their incisors in the supine position on the intubating platform. Curved blunt-ended forceps were used to carefully open the mouth and grasp the tongue, allowing the PE-10 tubing to be inserted into the trachea to instill the samples. The mice were maintained in the supine position on the intubating platform for at least 30 s. Thereafter, the mice were placed prone on a heating pad for recovery. Mice survival and body weight were recorded over time and presented using Kaplan–Meier curves (n = 14). A sham group without CLP and a CLP group without the *P. aeruginosa* challenge were applied as control groups. The CLP mice were monitored twice daily, and their conditions were evaluated using a sepsis scoring sheet. The moribund animals with a murine sepsis score above 21 were euthanized before spontaneous death[53].

MRSA and *P. aeruginosa*-induced polymicrobial blood infection model. Mice were infected with 0.1 ml bacterial suspension (mixed MRSA (ATCC 33591) and *P. aeruginosa* with 5×10^7 CFU for each pathogen) through a tail vein injection. Six hours after infection, the mice were grouped randomly and intravenously injected with various formulations including PBS, NAD$^+$-LP-CaP, free Rif, Rif-LP-CaP and NAD$^+$-Rif-LP-CaP (20 mg kg^{-1} NAD$^+$ and 10 mg kg^{-1} Rif; n = 10). The survival and body weight of the mice were recorded over time.

CFU detection. In the MRSA and *P. aeruginosa*-induced polymicrobial blood infection model, twelve hours after bacteria inoculation, the animals (n = 6) were euthanized by CO$_2$ asphyxiation. Blood and major organs (that is, liver, spleen, lungs, kidneys) were collected and homogenized in 3 ml PBS. The CFUs in the blood and infected organs were determined by serial dilution and plate counting.

Histopathological analysis. Organ injury in the polymicrobial infection model was evaluated by blood biochemistry and histological analysis. Twenty-four hours after bacterial inoculation, the animals with different treatments (n = 3) were killed, and their blood was collected for blood biochemistry tests. Major organs were harvested and sectioned. Haematoxylin and eosin staining was carried out for histological examinations. A TUNEL assay was performed on tissue sections using a chromogenic kit (catalog. no. A049, ABP Biosciences).

Statistical analysis. Results are presented as mean ± s.d. Assignments of the mice to treatments and selections of fields of microscopic inspection were made at random. Differences between the experimental groups were assessed using a one-way ANOVA test followed by Tukey's post hoc comparison test. The survival benefit was determined using a log-rank test. Experiments were repeated multiple times as independent experiments, as indicated in the figure captions. Analyses were performed using GraphPad Prism software. $P < 0.05$ was considered to be statistically significant in all analyses (95% confidence level).

Reporting summary. Further information on research design is available in the Nature Research Reporting Summary linked to this article.

Data availability
The authors declare that data supporting the findings of this study are available within the article and its Supplementary Information files. All relevant data are available from the corresponding author upon reasonable request.

References
49. Sendler, M. et al. Cathepsin B-mediated activation of trypsinogen in endocytosing macrophages increases severity of pancreatitis in mice. *Gastroenterology* **154**, 704–718.E10 (2018).
50. Vong, L., Sherman, P. M. & Glogauer, M. in *Mouse Models of Innate Immunity* (ed. Allen, I. C.) 41–50 (Springer, 2013).
51. Livak, K. J. & Schmittgen, T. D. Analysis of relative gene expression data using real-time quantitative PCR and the 2$^{-\Delta\Delta C_T}$ method. *Methods* **25**, 402–408 (2001).
52. Dawulieti, J. et al. Treatment of severe sepsis with nanoparticulate cell-free DNA scavengers. *Sci. Adv.* **6**, eaay7148 (2020).

Corresponding author(s): Shaoqin Gong

Last updated by author(s): Mar 6, 2022

Reporting Summary

Nature Portfolio wishes to improve the reproducibility of the work that we publish. This form provides structure for consistency and transparency in reporting. For further information on Nature Portfolio policies, see our Editorial Policies and the Editorial Policy Checklist.

Statistics

For all statistical analyses, confirm that the following items are present in the figure legend, table legend, main text, or Methods section.

n/a	Confirmed	
☐	☒	The exact sample size (*n*) for each experimental group/condition, given as a discrete number and unit of measurement
☐	☒	A statement on whether measurements were taken from distinct samples or whether the same sample was measured repeatedly
☐	☒	The statistical test(s) used AND whether they are one- or two-sided *Only common tests should be described solely by name; describe more complex techniques in the Methods section.*
☒	☐	A description of all covariates tested
☐	☒	A description of any assumptions or corrections, such as tests of normality and adjustment for multiple comparisons
☐	☒	A full description of the statistical parameters including central tendency (e.g. means) or other basic estimates (e.g. regression coefficient) AND variation (e.g. standard deviation) or associated estimates of uncertainty (e.g. confidence intervals)
☐	☒	For null hypothesis testing, the test statistic (e.g. *F*, *t*, *r*) with confidence intervals, effect sizes, degrees of freedom and *P* value noted *Give P values as exact values whenever suitable.*
☒	☐	For Bayesian analysis, information on the choice of priors and Markov chain Monte Carlo settings
☒	☐	For hierarchical and complex designs, identification of the appropriate level for tests and full reporting of outcomes
☒	☐	Estimates of effect sizes (e.g. Cohen's *d*, Pearson's *r*), indicating how they were calculated

Our web collection on statistics for biologists contains articles on many of the points above.

Software and code

Policy information about availability of computer code

Data collection	Data were collected using the software of the instrument described in each experiment. Flow cytometry data were collected using Attune NxT software 4.2; In vivo imaging data were collected using Spectrum Living Image 4.0 Software; Confocal microscopy data were collected using Nikon A1R confocal microscope (NIS-Elements V5.2); Plates were read by Progmega GloMax; DLS analysis was collected using Zetasizer software 7.02; qPCR data were collected using CFX Manager Software 3.0.
Data analysis	Excel and GraphPad Prism (9.0) was used for statistical analysis; FlowJo (10.1) was used for flow cytometry data analysis; Living Image software (v4.0) for IVIS images; Zetasizer (7.02) for DLS data; CFX Manager Software 3.0 for qPCR data.

For manuscripts utilizing custom algorithms or software that are central to the research but not yet described in published literature, software must be made available to editors and reviewers. We strongly encourage code deposition in a community repository (e.g. GitHub). See the Nature Portfolio guidelines for submitting code & software for further information.

Data

Policy information about availability of data

All manuscripts must include a data availability statement. This statement should provide the following information, where applicable:

- Accession codes, unique identifiers, or web links for publicly available datasets
- A description of any restrictions on data availability
- For clinical datasets or third party data, please ensure that the statement adheres to our policy

> All data generated or analyzed for this study are included in this published article and its supplementary information files.

Field-specific reporting

Please select the one below that is the best fit for your research. If you are not sure, read the appropriate sections before making your selection.

☒ Life sciences ☐ Behavioural & social sciences ☐ Ecological, evolutionary & environmental sciences

For a reference copy of the document with all sections, see nature.com/documents/nr-reporting-summary-flat.pdf

Life sciences study design

All studies must disclose on these points even when the disclosure is negative.

Sample size	Pilot studies were used for estimation of the sample size required to ensure adequate power. In vitro experiments were performed with at least 3 replicates, and the sample sizes for the in vivo experiments are listed as below: For the in vivo biodistribution studies, n=3. For the LPS-induced sepsis mouse survival studies, n=10. For the quantification of proinflammatory cytokine and inflammation-related gene expression in mouse blood, n=6. For the lung vascular permeability measurements, n=6. For the in vivo flow cytometry studies, n=5. For the CLP and secondary infection model, n=10 for the sham group, while n=14 for all other treatment arms. For the polymicrobial blood infection model, n=10. For the in vivo bacterial CFU studies, n=6. For the histopathological analysis, n=3.
Data exclusions	None
Replication	Experiments were replicated independently for at least three times with similar results.
Randomization	Throughout the whole experiment, samples and animals were randomized into groups.
Blinding	Blinding was not performed since all data reported were objectively measurable data. All samples were treated in the same manner for each experiment.

Reporting for specific materials, systems and methods

We require information from authors about some types of materials, experimental systems and methods used in many studies. Here, indicate whether each material, system or method listed is relevant to your study. If you are not sure if a list item applies to your research, read the appropriate section before selecting a response.

Materials & experimental systems

n/a	Involved in the study
☐	☒ Antibodies
☐	☒ Eukaryotic cell lines
☒	☐ Palaeontology and archaeology
☐	☒ Animals and other organisms
☒	☐ Human research participants
☒	☐ Clinical data
☒	☐ Dual use research of concern

Methods

n/a	Involved in the study
☒	☐ ChIP-seq
☐	☒ Flow cytometry
☒	☐ MRI-based neuroimaging

Antibodies

Antibodies used	The antibody information is listed as below, written with the order of antibody name, fluorophore, clone, company, cat number and lot number:

1. CD45, BB515, 30-F11, BD Biosciences, 564590, 9301305
2. CD11b, PE-Cy5, M1/70, Tonbo Biosciences, 55-0112-U100, C0112071619553;
3. Ly6C, APC, HK1.4, Biolegend, 128016, B274371;
4. Ly6G, Violet Fluor 500, 1A8, Tonbo Biosciences, 85-1276-U100, C1276101719853;
5. CD3, PE-Cy7, 145-2C11, Tonbo Biosciences, 60-0031-U100, C0031030119603;
6. CD8, Alexa Fluor 700, 53-6.7, Biolegend, 100730, B285812;
7. CD4, Violet Fluor 450, RM4-5, Tonbo Biosciences, 75-0042-U100, C0042030920753;
8. Annexin V, PE, n/a, Tonbo Biosciences, 50-6409-T100, C6409100218503;
9. CD45, PE, 30-F11, Tonbo Biosciences, 50-0451-U100, C0451092120503.
10. Annexin V, FITC, n/a, Tonbo Biosciences, 35-6409-T100, C6409012820353
11. ASC, Alexa Fluor 488, n/a, Santa Cruz Biotechnology, sc-514414, A2221
12. NF-κB, Alexa Fluor 488, n/a, Santa Cruz Biotechnology, sc-8008, K1020
13. VE-cadherin, Alexa Fluor 488, n/a, Santa Cruz Biotechnology, sc-9989, I0920

Validation	All antibodies were verified by the supplier and each lot received quality test.

Eukaryotic cell lines

Policy information about cell lines

Cell line source(s)	Human embryonic kidney cells (HEK293): ATCC Human umbilical vein endothelial cells (HUVECs): ATCC Murine macrophage cell line (RAW 264.7): ATCC
Authentication	HEK293, HUVEC and RAW264.7 cells are commercial cell lines and authenticated by the vendors.
Mycoplasma contamination	All cell lines were tested for mycoplasma contamination every month of culture.
Commonly misidentified lines (See ICLAC register)	HEK293 cell line is different to HEK (registration ID ICLAC-00063), which carries a separate genetic identity. See ATCC catalog for STR profiles of HeLa (CCL-2) and HEK-293 (CRL-1573).

Animals and other organisms

Policy information about studies involving animals; ARRIVE guidelines recommended for reporting animal research

Laboratory animals	BALB/c (8-12 weeks, female, The Jackson Laboratory) mice were used for the in vivo experiments.
Wild animals	This study did not involve wild animals.
Field-collected samples	The study did not involve samples collected from field.
Ethics oversight	All animal experiments were performed under the Guide for the Care and Use of Laboratory Animals (National Institutes of Health) and protocol (M006127) approved by the Institutional Animal Care and Use Committee (IACUC) at the University of Wisconsin.

Note that full information on the approval of the study protocol must also be provided in the manuscript.

Flow Cytometry

Plots

Confirm that:

☒ The axis labels state the marker and fluorochrome used (e.g. CD4-FITC).

☒ The axis scales are clearly visible. Include numbers along axes only for bottom left plot of group (a 'group' is an analysis of identical markers).

☒ All plots are contour plots with outliers or pseudocolor plots.

☒ A numerical value for number of cells or percentage (with statistics) is provided.

Methodology

Sample preparation	Single cell suspensions from cultured cells or mouse blood or tissues were used for flow cytometry tests. Immune cells in the lungs and spleen were isolated by squeezing through a 70-μm nylon mesh to create the single cell suspension. Red blood cells in the samples were lysed using ACK buffer (BioWhittaker) and cells were washed with PBS twice.
Instrument	Attune NxT Cytometer
Software	Attune™ NxT Software and FlowJo X
Cell population abundance	No post-sort fractions were collected.

Gating strategy | Cell debris and doublets were excluded by the forward and side scatter parameters (FSC, SSC) as exemplified in Supplementary Fig. 24.

☒ Tick this box to confirm that a figure exemplifying the gating strategy is provided in the Supplementary Information.